A Study of the Internal Two-Phase Flow in Gas-Centered Swirl Coaxial Injectors

Moongeun Hong[1], Jean-Philippe Matas[2], Sylvain Marty[2], Alain Cartellier[2], Soo Yong Lee[1], Antoine Delon[2]

[1]*Advanced Rocket Research Team, Korea Aerospace Research Institute, Daejeon, Korea*
[2]*Laboratoire des Ecoulements Géophysiques et Industriels (CNRS/UJF/Grenoble INP), Grenoble, France*

Keywords: gas-centered swirl coaxial injector, dynamic pressure ratio, swirl strength, interfacial instability, atomization, liquid film

Abstract

An effective atomization of liquid is of importance in the performance of combustion engines. For liquid hydrocarbon rocket engines with a staged combustion cycle for high-power application, the Gas-Centered Swirl Coaxial (GCSC) injector is widely employed. Gaseous oxidizer at high velocity enters directly through the center of the injector and is surrounded by a swirled liquid film injected along the periphery of the injection element. The swirled liquid film is stripped and fragmented into drops by the high velocity gas stream. The understanding of the atomization characteristics of the injector should be improved for the design of more reliable and efficient injectors dedicated to liquid rocket engines. In order to effectively evaluate atomization performances, it is essential to precisely predict liquid film dynamics inside the injector. The liquid film thickness and length are a function of the injector recess length, and they affect the atomized drop size. Internal flow visualization with a LIF (Laser Induced Fluorescence) method was conducted to investigate the overall form and the interface corrugation of the liquid flow at various swirl strength conditions. The swirl strength is varied by changing the inlet angle of tangential entry holes. The experimental results show clearly that the intact liquid length increases with increasing the swirl strength at the same dynamic pressure ratio. We also measured the frequency of the surface perturbations with a spectral method. We find that this frequency increases steadily with gas velocity, and appears to be independent of the initial swirl number.

1. Introduction

The break-up of a bulk liquid into droplets is an important phenomenon encountered across a wide range of industrial applications, and consequently a considerable amount of study has been conducted to understand various atomization mechanisms. Notably, the atomization phenomena in the application of liquid rocket engines have been actively studied to improve the injection system and thereby optimize combustion. However, various aspects of atomization characteristics of two-phase coaxial injectors, which are usually used for liquid rocket engines, are still not sufficiently understood. Moreover, most of the related studies have been focused on the atomization of a liquid jet or sheet by a concurrent gas flow. There are few studies on atomization of a swirled liquid film with one free and one wall-bounded surface. The atomization of a swirled liquid film occurs in liquid hydrocarbon rocket engines with a staged combustion cycle for high-power application. Swirled liquid hydrocarbon films are stripped and fragmented by a high velocity oxygen gas flow in the Gas-Centered Swirl Coaxial (GCSC) injectors. However, available results on the atomization characteristics of this injection configuration are too scarce to be helpful for design.

The dynamic pressure ratio, recess length and swirl strength are considered as main parameters in determining the overall spray characteristics of GCSC injectors (Lightfoot et al. 2007, 2008a, 2008b). For example, Jeon et al. (2011) proposed a critical dynamic pressure ratio to identify the flow patterns as internal or external mixing in the injectors. Concerning the interfacial instability, Harper et al. (2004) performed a numerical analysis to determine the unsteady hydrodynamic characteristics inside GCSC injectors and showed that the liquid interfacial frequency decreases as liquid film thickness and swirl velocity increase. Recently, Schumaker et al. (2011) studied the effect of swirl strength on the intact liquid film length inside the injectors. They showed that the liquid film length without liquid swirl is shorter than any of the cases with swirl when the total momentum flux ratio is less than 50. Moreover, they suggested the total momentum flux ratio could be used to scale the intact film length, and ultimately the atomization ratio and efficiency.

In order to improve the understanding of the atomization in GCSC injectors, we carry out a study on two-phase flow inside the injectors. The effect of the swirl strength on the intact liquid length is investigated by internal flow visualization. In addition, stability of the interface between the fast gas stream and the swirled liquid film is investigated via spectral measurement of the most unstable mode. First, the experimental setup and method are described. The effect of the swirl strength is then discussed, followed by the presentation of results on the frequency of the surface instability.

2. Experimental Methods

2.1 GCSC injectors

Figure 1 shows the experimental setup and the schematics of the GCSC injector used in the present study. In applications related to liquid rocket engines, gaseous propellant (GOX) at a high velocity enters direct through the center of the injector. Swirled liquid propellant (Kerosene) film is injected along the periphery of the injection element and then stripped and fragmented into drops by the high velocity gas stream. For cold flow tests, water and air are used as working fluids at atmospheric pressure.

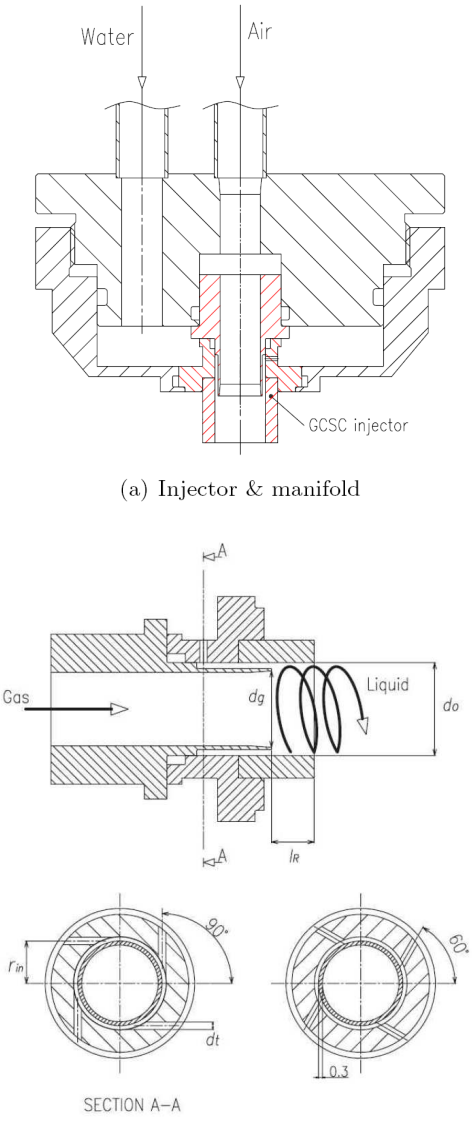

Figure 1: Experimental setup and GCSC injector schematics.

The injectors are made of acryl with an external shape of a regular tetragon in order to investigate the internal flow by visualization. Different diameters for gas flow at the end of sheltering lip d_g are investigated, namely 9.8, 10.4 and 10.8 mm. The outer diameter d_o of GCSC injectors is 12.4 mm and the lip thickness is 0.3 mm. Consequently, the heights of passage H_l become 0.5, 0.7 and 1.0 mm for d_g =10.8, 10.4 and 9.8 mm respectively. The diameter of the four liquid tangential entries d_t is 1.0±0.01 mm. The recess length l_R is a fixed value of 11.4 mm and the corresponding recess ratio l_R/d_o is 0.92. The volumetric liquid and gas flow rates are measured, and velocities used to calculate the dynamic pressure ratio. The uncertainty of the measured liquid and gas flow rates are less than 1 liter/hour and 10 Nl/min respectively.

Liquid swirl strengths are varied by changing the inlet angle α_{in} of entry holes as shown in Fig. 1(b). The swirl number S_w is usually defined by the ratio of the axial flux of angular momentum to axial linear momentum flux multiplied by the injector nozzle radius. However, for simplicity, the swirl number is defined by the ratio of the tangential velocity to the axial velocity when there is no recess; $S_w=u_{l\theta}/u_{la}$. The axial and tangential velocity can be obtained from measured spray angle and liquid mass flux conservation.

2.2 Internal flow visualization

Internal flow visualization with a LIF (Laser Induced Fluorescence) method was conducted to investigate the overall form and the interface corrugation of the liquid flow at various experimental conditions. For the experimental setup of the LIF system, a Coherent Innova 70 argon laser and optical lens are used to produce a laser sheet which was introduced along the central axis of the injector. A Phantom high speed digital camera is employed to capture images. Fluorescein is mixed with the liquid (water), and visualization of fluoresced light is carried out through an optical filter in order to remove any reflected or refracted light. The exposure time and the image number for each experimental condition are 99 μs (10,000 frames/s) and 7,000 respectively.

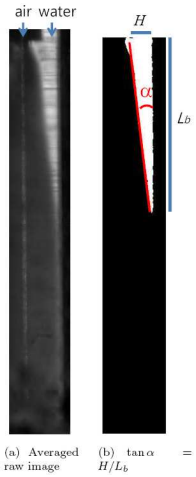

Figure 2: Image treatment and definition of α (H_l =0.5 mm, α_{in} =0°, M=2.07). Left: averaged raw image; right: thresholded image.

A digital image processing algorithm was developed with MATLAB to identify the intact liquid area inside the injectors. The 8-bit (0~255 level) gray-scaled raw images captured by the digital camera were averaged and then converted into binary image files using a proper threshold value. Otsu's method was employed for the reduction of a gray image to a binary image. This method calculates the threshold value which minimizes the interclass variance of the bi-modal histogram assumed from the gray level intensities (Otsu 1979). Once the binary image has been computed, the slope of the intact liquid area is calculated by

a simple linear regression with liquid interface points. The intact liquid length L_b can be derived from the cone angle α (refer to Fig. 2) by:

$$L_b = \frac{H}{\tan \alpha} \qquad (1)$$

Here, H represents a characteristic height of passage for the liquid inlet flow. From the images, this passage height is greater than the geometrical height, H_l and less than H_l+0.3 mm (lip thickness). The increase of H is due to the low pressure in the gas flow recirculation. However, for simplify, the axial liquid velocity is calculated based on H_l.

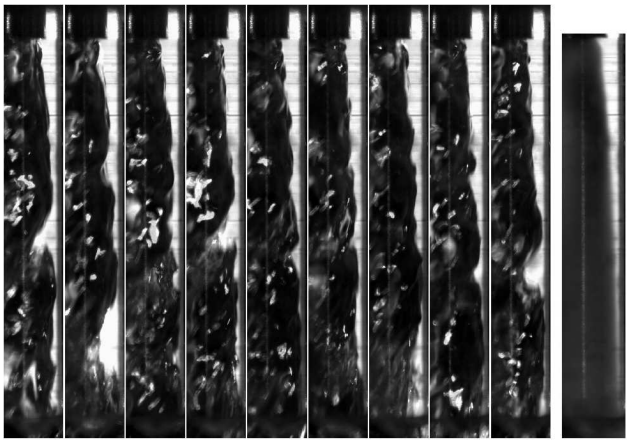

Figure 3: Raw images and the averaged image (H_l =0.5 mm, α_{in} =90°, u_{la}=1.4 m/s, M=1.83).

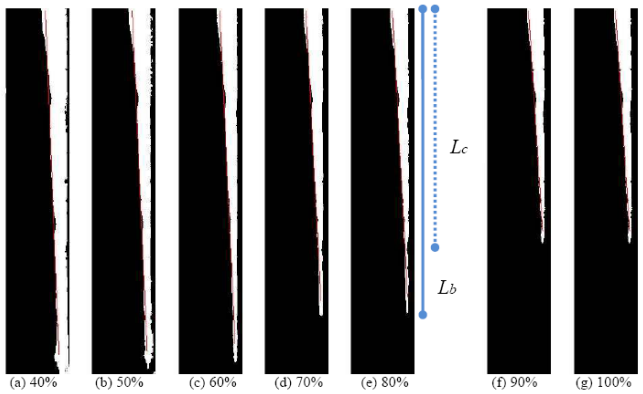

Figure 4: Binary images as a function of the threshold level: % means the percentage of Otsu's value (H_l =0.5 mm, α_{in} =90°, u_{la}=1.4 m/s, M=1.83).

For reliable measurements, the effects of the threshold level on the cone angle are investigated. Figure 4 shows the binary images obtained from the averaged image shown in Fig. 3 according to the threshold level from 40% to 100% of the Otsu's value. At low threshold values, the binary images are not able to appropriately represent the intact liquid area because waves or fragmented liquid inclusions connected to the intact liquid area are retained, and impair the slope calculation. On the other hand, for high threshold values, the intact liquid area quickly becomes partially perforated because of inhomogeneous light intensity inside the swirled liquid flow. Therefore, 80% of Otsu's value is chosen for the threshold level.

In addition to the threshold level, the effect of the range of intact liquid area (L_c in Fig. 4) is examined by varying from 50% to 100% of the raw L_b. Indeed, the difficulty here is to distinguish the conical zone without accounting for the remaining liquid film. L_c arises from the linear regression of the liquid cone angle. If L_c is too high, the cone angle intends to decrease because of the liquid film present at the end of the intact liquid area. However, for low L_c, the linear regression line may not be sufficient to properly represent the slope of the liquid interface because the line is calculated only over the forepart of the intact liquid area. Consequently, L_c is determined to be 80% of the raw L_b acquired from the binary image. The uncertainty of measurement in α is expected to be less than 0.3°.

We also look at the nature of surface perturbations: for a given downstream distance from liquid injection, we look at the variations of the thickness of the liquid stream as a function of time. A spectrum of this quantity is computed via MATLAB. We then observe that for certain conditions a clear maximum frequency dominates the spectrum (see figures 5 and 6 for examples of spectra). This frequency is then measured as a function of gas and liquid velocities. For a range of conditions two maxima frequencies are observed (see figure 6): a lower one whose peak is very narrow, and a larger one whose peak is much broader. The variation of each of these maxima as a function of experimental conditions will be discussed in the following section.

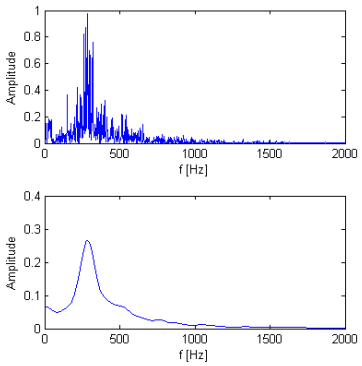

Figure 5: Examples of spectra of the interface perturbations, for u_g=39 m/s u_{la}=1 m/s and α_{in}=45°; top: spectrum of the whole set of images; bottom: the signal is split into 32 segments and averaged; the latter method is preferred when the spectrum is very noisy (see below).

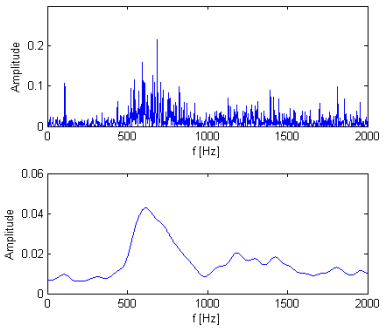

Figure 6: Spectrum obtained for u_g=94 m/s, u_{la}=1 m/s and α_{in}=45°: two maxima are observed, a broad one (for f =620 Hz) and a very thin one (f = 110 Hz).

3. Results and Discussion

3.1 Intact liquid length

The dynamic pressure ratio M ($=\rho_g u_g^2/\rho_l u_{la}^2$) is usually considered as a main parameter to determine the intact liquid length and the global spray characteristics of GCSC injectors. Figures 7 and 8 show the evolution of the internal liquid flow as a function of the dynamic pressure ratio at a constant liquid and gas velocity respectively. It is obviously shown that the intact liquid length decreases as the dynamic pressure ratio increases. Moreover, the global forms of the internal liquid flow are very similar to each other at the same value of M obtained from different combinations of liquid and gas velocities. The internal flow visualization at a same value of M is found in Fig. 9. Although the interfacial instability characteristics are different according to the gas and liquid velocities, it seems that the intact liquid length remains constant for the same M condition.

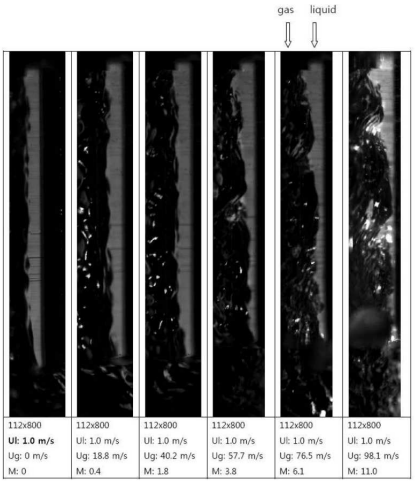

Figure 7: Evolution of the internal liquid flow as a function of the dynamic pressure ratio M at a constant u_{la}=1.0 m/s (H_l=0.7 mm, α_{in} =90°, M=0→11.0 from left to right).

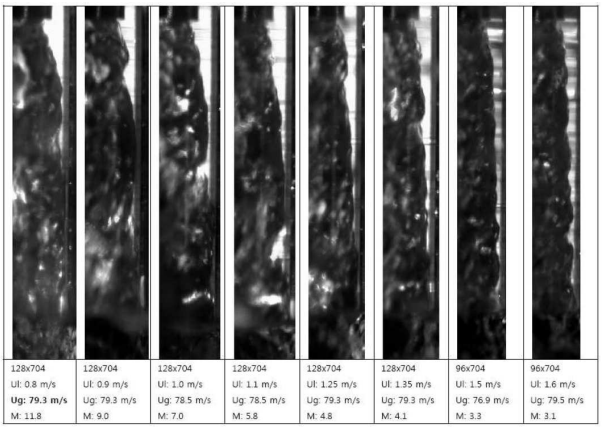

Figure 8: Evolution of the internal liquid flow as a function of the dynamic pressure ratio at a constant u_g=79 m/s (H_l =0.7 mm, α_{in} =90°, M=11.8→3.1 from left to right).

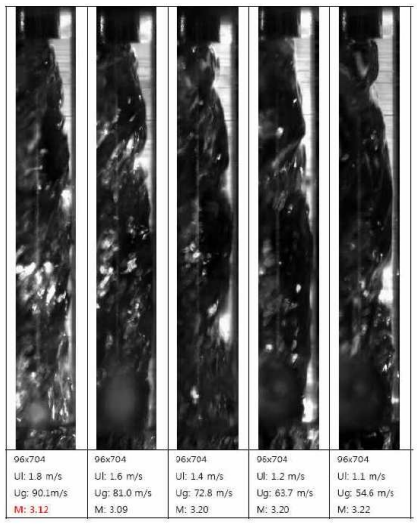

Figure 9: Evolution of the internal liquid flow at a constant M=3.1 obtained from different combinations of liquid/gas velocities (H_l=0.5 mm, α_{in}=90°, u_{la}=1.1~1.8 m/s, u_g=54.6~90.1 m/s).

Internal liquid flow evolutions according to the swirl strength are examined by changing the inlet angle of entry holes, α_{in}. Figures 10 and 11 show the variation of the internal liquid flow at various inlet entry angles for a same set of axial velocity conditions. Compared with the case of S_w=0 (α_{in}=0°), the intact liquid length increases when the swirl strength increases. For a same M, the intact liquid length reaches the end of the injector at S_w=2.2 (α_{in}=90°). Yet, the intact liquid length only slightly decreases when the swirl effect disappears. From the images, it seems that the interfacial wavelength and the amplitude of undulations decrease as the swirl strength increases.

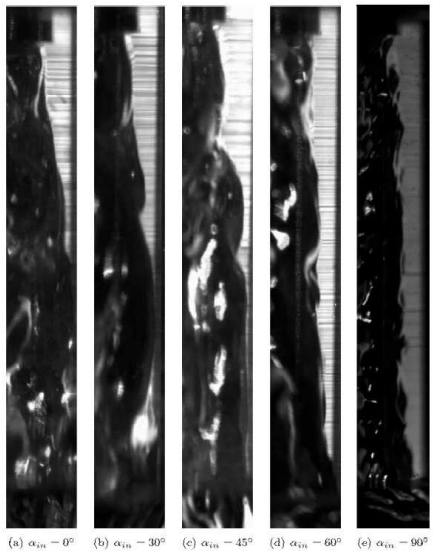

Figure 10: Variation of the internal liquid flow as a function of the swirl strength at a constant M=1.8 (u_{la}=1.0 m/s, u_g=39.2 m/s, H_l=0.7 mm, S_w=0, 0.4, 0.3, 2.0, 2.2 from left to right).

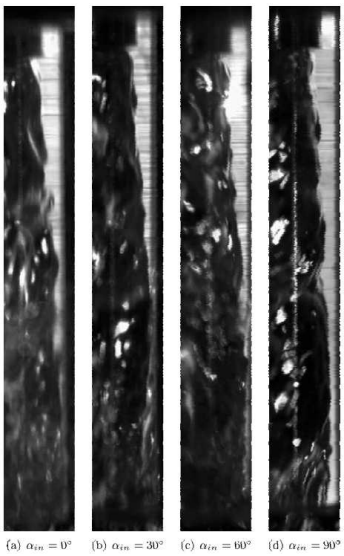

Figure 11: Evolution of the internal liquid flow as a function of the swirl strength at a constant M=1.46 (u_{la}=1.4 m/s, u_g=49.1 m/s, Hl=0.5 mm, Sw=0, 0.2, 1.3, 2.2 from left to right).

Figure 12 shows the effects of the dynamic pressure ratio and the swirl strength on the intact liquid length. As the dynamic pressure ratio increases and the swirl strength decreases, the intact liquid length somewhat decreases. Figure 12 demonstrates a power law dependency between the intact liquid length and the dynamic pressure ratio. As the swirl velocity increases, the liquid film becomes more stable, being forced against the injector inner wall with the increment of the azimuthal momentum. Consequently, the swirl reduces the atomization rate of the liquid film by increasing the intact liquid length. Regarding the effect of the swirl on the intact liquid length, Schumaker et al. (2011) suggested the total dynamic pressure ratio Mt ($=\rho_g u_g^2/\rho_l u_{l\alpha}^2(1+S_w^2)$) for scaling the intact liquid length. However, any significant relationship between the intact liquid length and the total dynamic pressure ratio is not found in the present study. Finally, it must be noted that the decrease of the intact liquid length as $M^{-1.2}$ observed here is steeper than the decrease in $M^{-1/2}$ observed in mixing layer experiments (Eggers & Villermaux 2008), and which is attributed to stripping of the liquid by the fast gas stream. We think that in the present case the thickness of the liquid stream is mainly driven by the acceleration of the liquid by the fast gas stream, which leads to thinning of the liquid film. Indeed, extra measurements (not shown here) indicate that few droplets are detached from the film so that the mass loss due to stripping is quite weak. Note that at large M values, where stripping becomes more efficient, the $M^{-1/2}$ dependency may eventually be recovered (see lower slope for M>2 on figure 12). Experiments at higher M are needed to confirm this point.

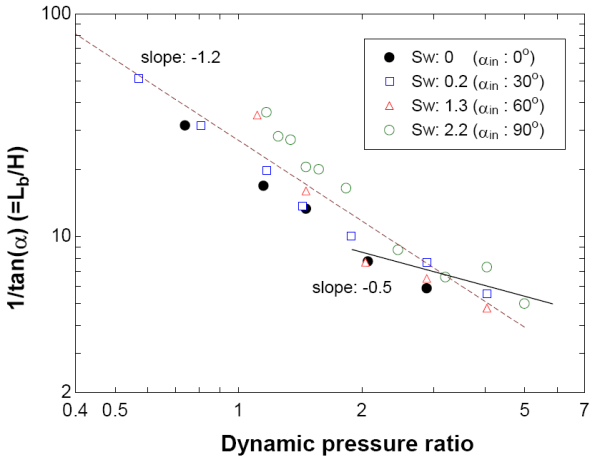

Figure 12: Variation of the intact liquid length as a function of the dynamic pressure ratio, or momentum flux ratio, for various swirl strengths (Hl=0.5 mm, d_g=10.8 mm).

3.2 Interfacial instability

Figures 13 to 17 show the variations of the most unstable frequency in surface perturbations, as a function of gas velocity. The error bars are related to the uncertainty on localizing the maximum in the spectrum, typically the width of the maximum peak in the spectrum.

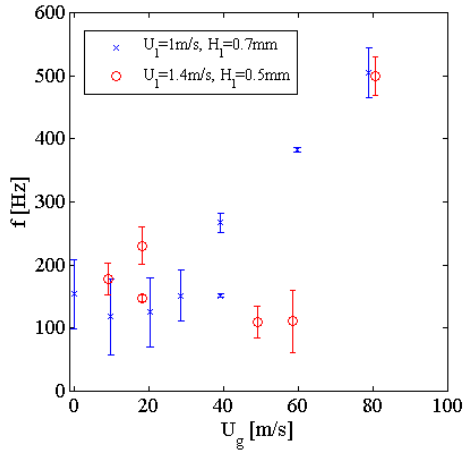

Figure 13: Variation of the frequency of the surface instability as a function of the gas velocity (αin =0°).

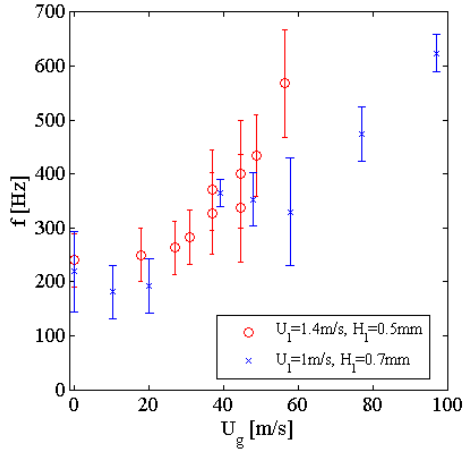

Figure 14: Variation of the frequency of the surface instability as a function of the gas velocity (αin =30°).

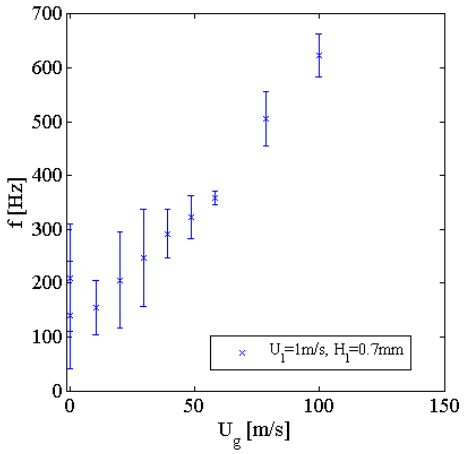

Figure 15: Variation of the frequency of the surface instability as a function of the gas velocity (αin =45°).

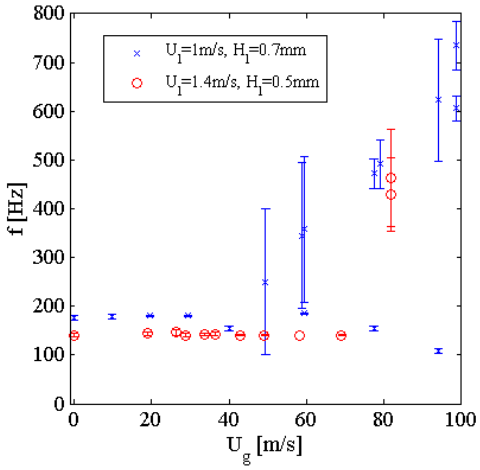

Figure 16: Variation of the frequency of the surface instability as a function of the gas velocity (αin =60°).

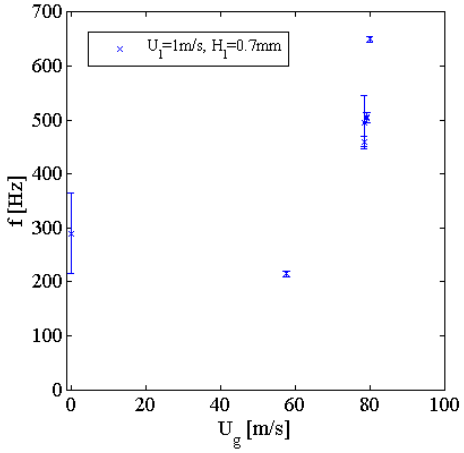

Figure 17: Variation of the frequency of the surface instability as a function of the gas velocity (αin =90°).

Frequency increases steadily as a function of gas velocity, for all injector conditions (i.e. for all initial swirl in the system). This is consistent with shear instabilities in mixing layers, where the frequency of the instability is mostly controlled by velocity of the gas phase; see for example Eggers & Villermaux (2008) for a review of shear instabilities in liquid jets. However a peculiar feature of the instability in the present study can be seen in figure 16, where two frequencies seem to actually coexist: in addition to the frequency increasing with ug, there is a constant frequency, comprised between 150 Hz and 200 Hz for the large range of gas velocities investigated. While the spectrum associated with the larger frequency is usually broad, the maximum associated with this lower frequency independent of ug is very narrow. Figure 6 shows an example of a spectrum where both frequencies coexist.

Figure 18 shows the superposition of the data for all αin and for Hl=0.7 mm: surprisingly it can be seen that the frequency does not vary much when the swirl is varied, and the collapse of the data is relatively good. Only the data for αin=90° (symbol *) departs a bit from the common curve: this is because of the occasional presence of a low frequency. The collapse is mostly observed for the higher frequency, increasing with ug; for Hl=0.7mm, the lower constant frequency is almost only present in figure 16, but note however that these points are roughly aligned with the couple of points for αin=0° and αin=90°, at $f \approx$ 200 Hz, which depart from the steadily increasing curve.

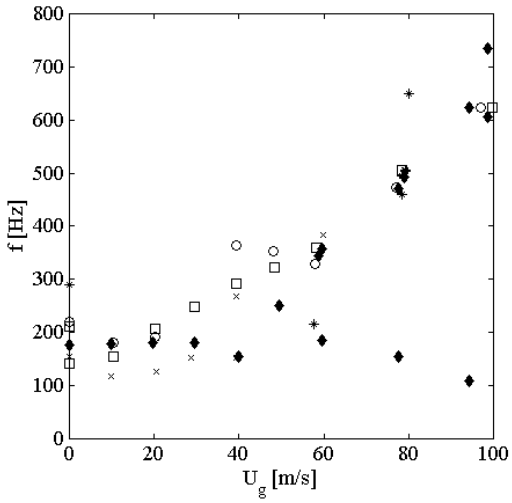

Figure 18: Variation of the frequency of the surface instability as a function of the gas velocity, for Hl =0.7 mm and for all αin investigated: x αin =0°; o αin =30°; □ αin =45°; ♦ αin =60°;* αin=90°.

In planar shear layer it is known that the two-phase shear instability is controlled by the thickness of the gas vorticity layer δ (Marmottant & Villermaux 2004, Matas et al 2011). More precisely, the frequency of the instability can be estimated from the ratio of the wave velocity Uc to the wavelength λ: wave velocity is the velocity of the frame in which dynamic pressure in both phases are balanced, $Uc \approx \sqrt{r}ug$ where r is the density ratio $r=\rho g/\rho l$; λ can be shown to be directly proportional to δ: $\lambda \approx \delta/\sqrt{r}$ (Marmottant & Villermaux 2004). This leads to a frequency scaling as $f \approx rug/\delta$. This estimate is valid when the dynamic pressure ratio is large, which may not be the case for the lower ug investigated here. Nonetheless comparison can be made between this prediction and our experimental values: gas vorticity thickness δ has been determined via hotwire measurements (with single sensors normal probe with 1.25 mm long and 0.5 μm in diameter, 55P11 of DANTEC Dynamics), and was found to follow $\delta \approx dgRe^{-1/7}$ for the conditions of our experiment. This yields frequencies in the

range 1 – 10 Hz, quite below the frequency observed experimentally. A different mechanism may be at play in the present configuration. In particular, we suspect the thickness of the liquid film affect the shear instability, since Hl is much smaller than the wavelength (see figure 8). Any future stability analysis would have to include the influence of this small Hl.

4. Conclusions

A study on the two-phase flow in the gas-centred swirl coaxial injector is carried out to investigate the effect of the swirl strength on the intact liquid length by the internal flow visualization. It is clearly shown that the intact liquid length decreases, in other words, the atomization rate increases as the swirl strength decreases and the dynamic pressure ratio increases. However, future work is needed to improve the understanding of the swirl effect on the intact liquid length. A frequency instability is observed on the liquid issued from the injector. This frequency increases with gas velocity, and does not appear to depend on the initial swirl number. This frequency is much larger than the inviscid frequency observed in classical mixing layer experiments. This is probably due to our having a very thin liquid stream in the present configuration.

Acknowledgements

We acknowledge financial support from the Egide/NRF PHC Star program, as well as from the French Agence Nationale de la Recherche (ANR) under reference ANR-2010-BLAN-0903 VAA.

References

Eggers, J. & Villermaux, E., "Physics of liquid jets", *Rep. Prog. Phys.* 71 036601 (2008).

Harper, B., Canino, J., Heister, S.D. & Carrison, L.A., "Hydrodynamic modelling of oxidizer-rich staged combustion injector flow," 52nd JANNAF Joint Propulsion Meeting, Las Vegas, NY (2004).

Jeon, J., Hong, M., Han, Y.-M. & Lee, S.Y., "Experimental study on spray characteristics of gas-centered swirl coaxial injectors," *J. Fluid Eng.-Trans. of ASME*, Vol. 133, 121303, (2011).

Lightfoot, M.D.A, Danczyk, S.A. & Talley, D.G., "A method to predict atomization performance in gas-centered swirl-coaxial injectors," 20th Annual Conference on Liquid Atomization and Spray Systems, Chicago, IL (2007).

Lightfoot, M.D.A, Danczyk, S.A. & Talley, D.G., "Atomization rate of gas-centered swirl-coaxial injectors," 21st Annual Conference on Liquid Atomization and Spray Systems, Orlando, FL (2008a).

Lightfoot, M.D.A, Danczyk, S.A. & Talley, D.G., "Scaling of gas-centered swirl-coaxial injectors," Technical Report, Air Force Research Laboratory, Edwards AFB, CA (2008b).

Marmottant, P. & Villermaux, E., "On Spray Formation", *J. Fluid Mech.*, 498, 73 (2004).

Matas, J.-P., Marty S. & Cartellier, A., "Experimental and analytical study of the shear instability of a gas-liquid mixing layer", *Phys. Fluids*, 23 094112 (2011).

Otsu, N., "A threshold selection method from gray-level histogram," *IEEE Trans. on System, Man and Cybernetics*, Vol. 8, pp. 62-66 (1979).

Schumarker, S.A., Danczyk, S.A. & Lightfoot, M.D.A., "Effect of swirl on gas-centered swirl-coaxial injectors," AIAA 2011-5621, 47th AIAA/ASME/SAE/ASEE Joint Propulsion Conference & Exhibit, San Diego, CA (2011).